Proceedings of the ASME 2012 31st International Conference on Ocean, Offshore and Arctic Engineering
OMAE2012
July 1-6, 2012, Rio de Janeiro, Brazil

OMAE2012-83581

A NONLINEAR EXTENSION FOR LINEAR BOUNDARY ELEMENT METHODS IN WAVE ENERGY DEVICE MODELLING

Alexis Merigaud
Dept. of Energy and Environment
ENSTA ParisTech
75015 Paris, France
Email: alexis.merigaud@ensta-paristech.fr

Jean-Christophe Gilloteaux
Integration Engineering Laboratory
Direction mécanique appliquée
IFP Energies nouvelles
1 et 4 avenue de Bois-Prau 92852
Rueil-Malmaison Cedex - France
Email: jean-christophe.gilloteaux@ifpen.fr

John V. Ringwood*
Centre for Ocean Energy Research
NUI Maynooth
Maynooth, Co. Kildare, Ireland
john.ringwood@eeng.nuim.ie

ABSTRACT

To date, mathematical models for wave energy devices typically follow Cummins equation, with hydrodynamic parameters determined using boundary element methods. The resulting models are, for the vast majority of cases, linear, which has advantages for ease of computation and a basis for control design to maximise energy capture. While these linear models have attractive properties, the assumptions under which linearity is valid are restrictive. In particular, the assumption of small movements about an equilibrium point, so that higher order terms are not significant, needs some scrutiny. While this assumption is reasonable in many applications, in wave energy the main objective is to exaggerate the movement of the device through resonance, so that energy capture can be maximised. This paper examines the value of adding specific nonlinear terms to hydrodynamic models for wave energy devices, to improve the validity of such models across the full operational spectrum.

NOMENCLATURE

$\vec{X}$ Wave energy device displacement
M Mass of wave energy device
$\vec{F}_i$ Force i on body
ϕ_i Potential flow i
P_i Pressure i on body
ρ Water density
z Displacement in heave (vertical) direction
C_{PTO} Power take off damping coefficient
K_i Convolution kernel i
η Free surface elevation
M_0 Mean body position
V_p Velocity at the center of panel p
τ_h^*, τ_h^{**} Second order force

1 INTRODUCTION

Environmental loads on wave energy converters arise essentially from waves, current and wind. In most cases, the operational and extreme loads are due to waves. A number of general theoretical formulations, which have been developed for application to seakeeping of ships and offshore structures and for coastal engineering problems, may be useful for analyzing wave energy devices. Among them, frequency-domain potential theory-based methods are commonly used for assessing offshore structures, which is the main reason why they have been extensively used for studying the problem of wave energy converters in waves [1–4]. However, this approach is meaningful only if the response of the system is linear, and significant differences are often observed between the results obtained by these numerical tools and experiments [5], since wave energy converters are floating bodies which may experience large amplitude motions and nonlinear responses. In fact, a major objective, in order to maximise the converted wave energy, is to exaggerate the motion of the device.

*Address all correspondence to this author.

In wave energy, three distinct families of time-domain models, based on boundary element hydrodynamic descriptions, may be distinguished based on their degree of complexity for computing the hydrodynamic loads. We note that, while linear models may be formulated in either the time- or frequency-domains, nonlinear models require a time-domain setting.

Linear method A first degree of complexity assumes that the body motion amplitude and the steepness of the waves are small. Hence, the boundary value problem (BVP) for the fluid potential can be linearised and all the quantities of interest can be expressed in terms of the mean wetted surface of the body. The diffraction-radiation forces acting on the body can be written as convolution products of impulse response functions (IRFs) with the velocity of the body (radiation forces) or with the free surface elevation associated with the incident wave (diffraction forces) [6]. Classically, commercial software such as WAMIT or AQUAPLUS are used. However, this approach is subject to the same limitations as in the frequency domain, and may therefore erroneously estimate the motion behaviour, when motion amplitude becomes significant.

Nonlinear improvement 1 A second degree of complexity, assumes that the Froude-Krylov force (i.e the sum of the incident wave force plus the Archimedes' thrust) is the main component of the hydrodynamic force. Hence, in order to improve the accuracy of the model, the integration of the incident wave pressure and the calculation of the hydrostatic force can be performed over the exact instantaneous wetted surface at each time step instead of the mean wetted surface, the wetted surface being defined as the surface of the moving hull underneath the undisturbed incident free-surface. Few models based on this theory have been applied in wave energy yet [7, 8], but show promising results.

Nonlinear improvement 2 In a third degree of complexity, the BVP is solved on the exact wetted surface. The difference with the previous method is that the free-surface conditions are no longer linearised around the mean water surface but are satisfied on the undisturbed free surface, assuming that the diffracted and radiated waves are small in comparison with the incoming wave field. This approach is known as the weak-scatter formulation of the BVP, and has been applied for the design of an autonomous data buoy using wave energy to satisfy power requirements [9].

In this paper, we examine the benefit of using the more complex formulations for wave energy applications and, in particular, document the performance benefit traded off against computational complexity. We adopt a spherical wave energy absorber for our study, since such a shape will help to highlight the different calculations based on the various assumptions of wetted surface area. We also assume that the device is tethered to the seabed, with the power take-off in series with the motion of the device, which is constrained to vertical (heave) motion only, for clarity. Fig.1 shows the wave energy device configuration.

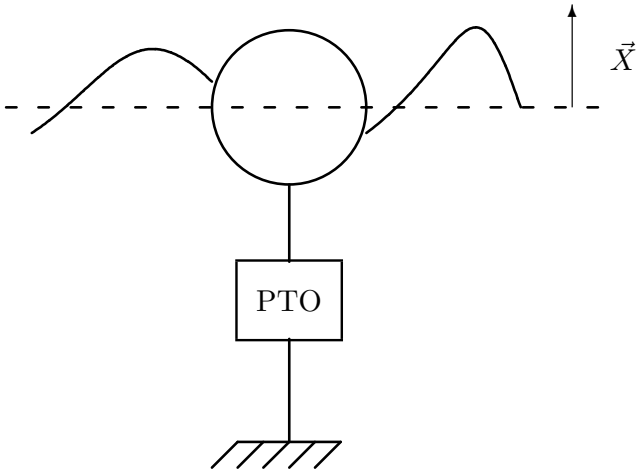

FIGURE 1. CONFIGURATION OF THE WAVE ENERGY DEVICE

2 General equations of motion

Initially, we consider a three-dimensional floating wave-energy device. We make the assumptions that the fluid is inviscid, and that the incident flow is irrotational and incompressible. We choose the physical space as an inertial frame of reference, normally taken to have its origin at the position of the gravity center of the body in its hydrostatic equilibrium position. Newton's law can now be used to specify the governing equation of motion, as follows:

$$M\ddot{\vec{X}} = \vec{F}_{gravity} - \iint_{body} P\,\vec{n}\,dS + \vec{F}_{PTO}, \tag{1}$$

where $\vec{X}$ is the position of the body relative to its hydrostatic equilibrium position, M the inertia matrix of the body, P is the pressure on an element dS of the body surface and $\vec{n}$ is a vector normal to the surface element, dS. $\vec{F}_{PTO}$ is the force associated with the power take-off which, for the present analysis, will be modelled as a simple linear damper, while $\vec{F}_{gravity}$ is the gravity force acting on the device.

The pressure, P, can be derived from the incident flow using Bernoulli's equation:

$$P = -\rho g z - \rho \frac{\partial \phi}{\partial t} - \rho \frac{|\nabla \phi|^2}{2} \tag{2}$$

The potential flow ϕ can be written as a sum of three potentials:

- ϕ_I the potential corresponding to the undisturbed incident flow,
- ϕ_{Diff} the diffracted potential, due to the presence of the body,
- ϕ_{Rad} the radiated potential, due to the motions of the body.

$$\phi = \phi_I + \phi_{Diff} + \phi_{Rad} \tag{3}$$

3 Forces acting on the body

Considering equations (2) and (3), the pressure can be written as follow:

$$\begin{aligned} P = & -\rho g z - \rho \frac{\partial \phi_I}{\partial t} - \rho \frac{|\nabla \phi_I|^2}{2} \\ & -\rho \frac{\partial \phi_{Diff}}{\partial t} - \rho \frac{|\nabla \phi_{Diff}|^2}{2} \\ & -\rho \frac{\partial \phi_{Rad}}{\partial t} - \rho \frac{|\nabla \phi_{Rad}|^2}{2} \\ & -\rho \nabla \phi_I \nabla \phi_{Rad} - \rho \nabla \phi_I \nabla \phi_{Diff} - \rho \nabla \phi_{Diff} \nabla \phi_{Rad} \end{aligned} \tag{4}$$

- $P_{stat} = -\rho g z$ is the static pressure. The static pressure force (Archimedes force) and the gravity force form the static Froude-Krylov force as:

$$\vec{F}_{FK_{stat}} = -\iint_{body} P_{stat} \vec{n} dS.$$

- $P_{dyn} = -\rho \frac{\partial \phi_I}{\partial t} - \rho \frac{|\nabla \phi_I|^2}{2}$ is the dynamic pressure, which generates the dynamic Froude-Krylov force as:

$$\vec{F}_{FK_{dyn}} = -\iint_{body} P_{dyn} \vec{n} dS.$$

- $P_{diff} = -\rho \frac{\partial \phi_{Diff}}{\partial t} - \rho \frac{|\nabla \phi_{Diff}|^2}{2}$ is the pressure associated with the diffracted potential. It generates the diffraction force:

$$\vec{F}_{Diff} = -\iint_{body} P_{diff} \vec{n} dS.$$

- $P_{rad} = -\rho \frac{\partial \phi_{Rad}}{\partial t} - \rho \frac{|\nabla \phi_{Rad}|^2}{2}$ is the pressure associated with the radiated potential. It generates the radiation force as:

$$\vec{F}_{Rad} = -\iint_{body} P_{rad} \vec{n} dS.$$

- $\rho \nabla \phi_I \nabla \phi_{Rad}$, $\rho \nabla \phi_I \nabla \phi_{Diff}$ and $\rho \nabla \phi_{Diff} \nabla \phi_{Rad}$ are second-order diffraction-radiation terms. In a first approximation, they will be neglected.

Eq. (1) can then be written as in (5), which allows the clear identification of the contributing individual forces, which will help in the classification of various modelling approaches.

$$M\ddot{\vec{X}} = \vec{F}_{FK_{stat}} + \vec{F}_{FK_{dyn}} + \vec{F}_{Diff} + \vec{F}_{Rad} + \vec{F}_{PTO} \tag{5}$$

A number of significant nonlinearities appear when one wants to solve the equations of motion, among them, in particular,

- the quadratic terms of Bernoulli's equation in (2),
- the incident potential flow, which can be nonlinear, and
- pressure forces which are integrated over the instantaneous wetted surface, thus creating geometric nonlinearities

Most models are based on linear approximations, obtained by the following assumptions:

- The quadratic terms are neglected,
- only linear waves are considered, and
- forces are integrated over the mean wetted surface

But such models, even though being very easy to use in control systems and often giving good approximations, are not always relevant in the case of wave energy absorbers. For example, linear simulations can result in the WEC body completely clearing the water, while the wetted surface is assumed to be constant! The calculation methods described in the following compute these terms more or less precisely and, of course, using more or less computation time. Ideally, we should be able to choose among these compromises, depending on the application.

4 Linear modelling

In the linear approach, the following procedure is followed:

Static Froude-Krylov forces (gravity and static pressure forces) are considered to act like a symmetrical mass-spring system: when the body is pushed down into the water, the Archimedes force pushes it up towards equilibrium and, for positive vertical excursions, gravity supplies the restoring force. The equivalent stiffness matrix of this mass-spring system is called the hydrostatic stiffness matrix, K_H, so that

$$\vec{F}_{FK_{stat}} = K_H \vec{X} \tag{6}$$

The linear radiation force is expressed as a convolution product according to Cummins decomposition [10]:

$$\vec{F}_{Rad} = -\mu_\infty \ddot{\vec{X}} - \int_{-\infty}^{\infty} K_{Rad}(t-\tau) \dot{\vec{X}}(\tau) d\tau \tag{7}$$

where μ_∞ is the added mass (at infinite frequency) and K_{Rad} the impulse-response matrix for the radiation force.

The dynamic Froude-Krylov and diffraction forces are computed together as an excitation force with a convolution

product, so that

$$\vec{F}_{FK_{dyn}} + \vec{F}_{Diff} = \vec{F}_{Ex} = -\int_{-\infty}^{\infty} K_{Ex}(t-\tau)\eta(0,0,\tau)d\tau \quad (8)$$

where K_{Ex} is the excitation impulse response matrix and η is the undisturbed free surface elevation at the center of the body.

The PTO force, for the purposes of this study, will be modelled as a linear damper, so that

$$\vec{F}_{PTO} = -C_{PTO}\dot{\vec{X}} \quad (9)$$

where C_{PTO} can be arbitrarily chosen.

5 Nonlinear improvement 1

In this approach, diffraction and radiation forces are still computed linearly. However, nonlinear Froude-Krylov forces are evaluated.

Static and dynamic Froude-Krylov forces are integrated over the instantaneous wetted surface:

$$\vec{F}_{FK} = \vec{F}_{FK_{stat}} + \vec{F}_{FK_{dyn}} = \vec{F}_{gravity} - \iint_{wetted\ surface} (P_{dyn} + P_{stat})\vec{n}dS \quad (10)$$

where P_{dyn} and P_{stat} are deduced from the incident potential flow as in equation (2). It requires a remeshing of the wetted surface at each time step, involving:

(a) Computation of the intersection between the body and the free surface,
(b) selection of the immersed or partially immersed panels, and
(c) remeshing of partially immersed panels through trans-finite elements methods as explained in [7].

Radiation forces are again linear and computed as in equation (7).

Diffraction forces remain linear as well but this time they are computed separately, since dynamic Froude-Krylov forces are computed at the same time as static Froude-Krylov forces. K_{Ex}, the impulse-response matrix for diffraction forces previously evaluated in Section 4, is used for the convolution product:

$$\vec{F}_{Diff} = -\int_{-\infty}^{\infty} K_{Ex}(t-\tau)\eta(0,0,\tau)d\tau \quad (11)$$

PTO forces remain the same as in Section 4.

6 Nonlinear improvement 2

This approach is similar to that in Section 5, except for diffraction forces which are computed more precisely, since the convolution product in (11) is performed on each point of the mean wetted surface:

$$\vec{F}_{Diff} = \sum_{j \in mean\,wetted\,surf} (-\int_{-\infty}^{\infty} K_j(t-\tau)\eta(x_j,y_j,\tau)d\tau) \quad (12)$$

The points of the mean wetted surface, their x- and y-coordinates and their associated diffraction impulse-response matrices have been previously computed by hydrodynamic software.

6.1 Diffraction-radiation forces: development up to second order

In the development so far, diffraction and radiation forces were assumed to be linear. However, from equation (4) a more precise expression for diffraction and radiation forces is:

$$\vec{F}_{Diff} + \vec{F}_{Rad} = \iint_{body} (-\rho\frac{\partial\phi_{Diff}}{\partial t} - \rho\frac{|\nabla\phi_{Diff}|^2}{2} - \rho\frac{\partial\phi_{Rad}}{\partial t} - \rho\frac{|\nabla\phi_{Rad}|^2}{2})dS \quad (13)$$

The linear diffraction and radiation forces computed as in (7) and (11) only correspond to a linear approximation of the time-derivative terms of (13). A more precise computation of these time-derivative terms can be obtained by expansion to second-order. As Gilloteaux [7] shows , a Taylor series expansion of the time derivative of the total potential and of the normal to the wetted surface can be performed around the mean position of the body. The following force is obtained:

$$\tau_h^*(t) = \iint_{S_0} [\partial x'\frac{\partial\phi_t}{\partial x'} + \partial y'\frac{\partial\phi_t}{\partial y'} + \partial z'\frac{\partial\phi_t}{\partial z'}]n(M_0')dM_0' + \iint_{S_0} [\frac{\partial\phi_t}{\partial t}]n(M_0')dM_0' \quad (14)$$

In addition to this, the following quadratic terms of Bernoulli's equation have not been taken into account yet: $\rho\frac{|\nabla\phi_{Diff}|^2}{2}$, $\rho\frac{|\nabla\phi_{Rad}|^2}{2}$, $\rho\nabla\phi_I\nabla\phi_{Rad}$, $\rho\nabla\phi_I\nabla\phi_{Diff}$ and $\rho\nabla\phi_{Diff}\nabla\phi_{Rad}$ (see Section 3). For these, following expression may be obtained:

$$\tau_h^{**}(t) = -\frac{\rho}{2}\iint_{S_0} |\nabla\phi_{\delta,p}\otimes V_p|^2 n_0 dS - \frac{\rho}{2}\iint_{S_0} |\nabla\phi_{\delta,p}\otimes V_I|^2 n_0 dS$$
$$-\rho\iint_{S_0} |\nabla\phi_{\delta,p}\otimes\nabla\phi_I||\nabla\phi_{\delta,p}\otimes V_p| n_0 dS$$
$$-\rho\iint_{S_0} \nabla\phi_I|\nabla\phi_{\delta,p}\otimes V_p| n_0 dS$$
$$-\rho\iint_{S_0} |\nabla\phi_{\delta,p}\otimes V_p||\nabla\phi_{\delta,p}\otimes\nabla\phi_I| n_0 dS \qquad (15)$$

where V_p is the velocity of the center of panel p and $\nabla\phi_{\delta,p}$ its potential gradient vector, computed by hydrodynamic software. Second-order terms τ_h^* and τ_h^{**} can be computed by the program in order to get even more precise results, if required.

7 Results

A custom program, written in Fortran and drawing on the ACHIL3D hydrodynamic software suite, was used to calculate the results. The overall program structure is shown in Fig.2. As can be seen from Fig.2, where possible, pre-processing is utilised to take fixed calculations out of the iterative simulation loop.

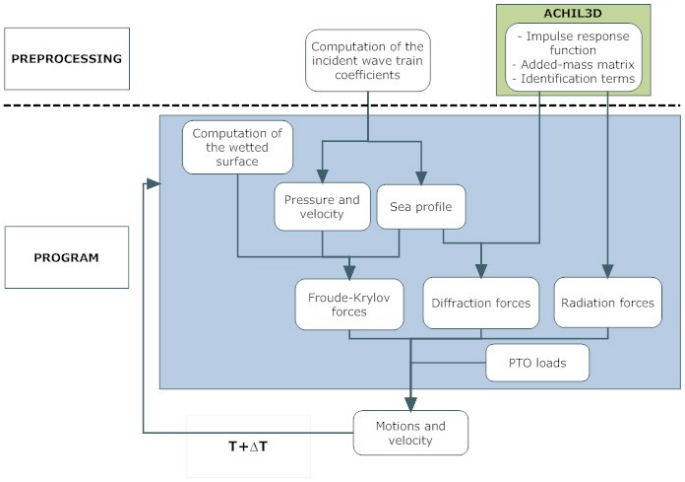

FIGURE 2. STRUCTURE OF SOFTWARE PROGRAM

For the results comparison, the device used was a sphere of 1m radius, with a (uniform) density of $500 kg.m^{-3}$. As we want to highlight the effects of nonlinearities, we worked with regular nonlinear waves (Rienecker-Fenton's waves [11]), with a 6s wave period. In order to assess realistic motions for a wave energy application, the PTO damper was optimised, using the linear model. This gave a value for $C_{PTO} = 27429 N.s.m^{-1}$ for a $6s$ wave period, bearing in mind that the optimal PTO damping is frequency sensitive.

7.1 Device motion

For these tests, a wave amplitude of 0.5m (1m peak-to-peak) was employed. Fig.3 shows the displacement and velocities for the linear and nonlinear models. Note that the 'nonlinear 1' corresponds to the formulation of Section 5, while 'nonlinear 2' corresponds to the formulation of Section 6. We can note that there is a significant difference between the nonlinear and linear responses, but a relatively insignificant difference between the two nonlinear approaches.

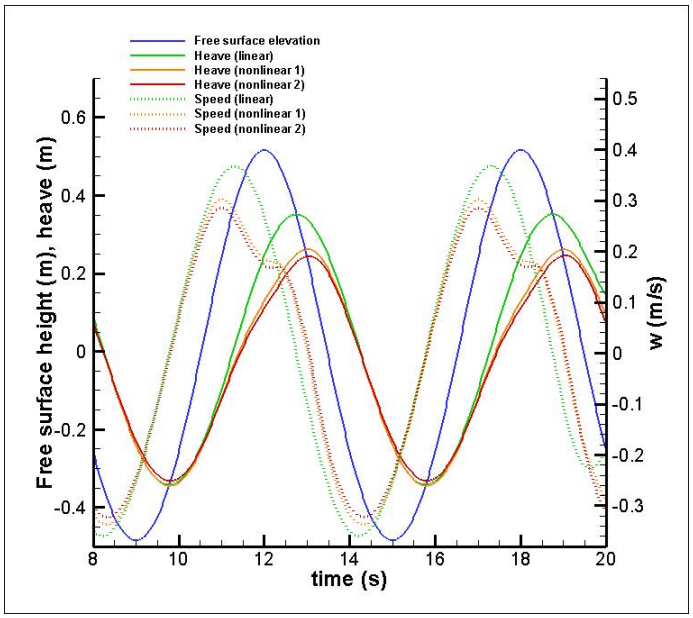

FIGURE 3. HEAVE DISPLACEMENT AND VELOCITY

In order to ascertain the root cause of the differences between linear and nonlinear approaches, we can individually examine each force in the formulation of eq. (5). Fig.4 shows the excitation forces, while Fig.5 shows the static Froude-Krylov forces.

We note that the excitation forces are mainly responsible for the first differences observed between linear and nonlinear simulations (at $t \approx 10.5 s$), as Fig.4 shows. Since the excitation forces are the sum of the dynamic Froude-Krylov and diffraction forces, and diffraction forces are computed linearly in the three methods, differences are accounted for by the dynamic Froude-Krylov forces. The peak at $t \approx 13.25 s$ can be accounted for by the PTO force and, to some extent, the radiation force (see Figs.6 and 7).

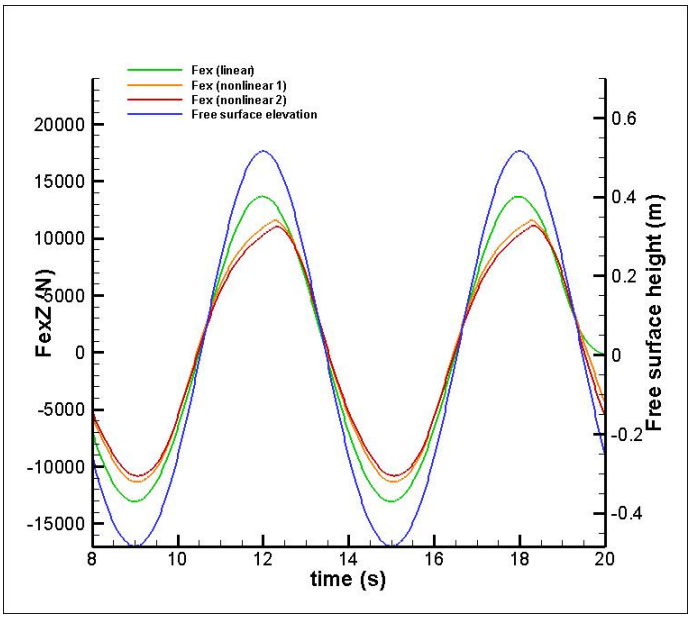

FIGURE 4. EXCITATION FORCE

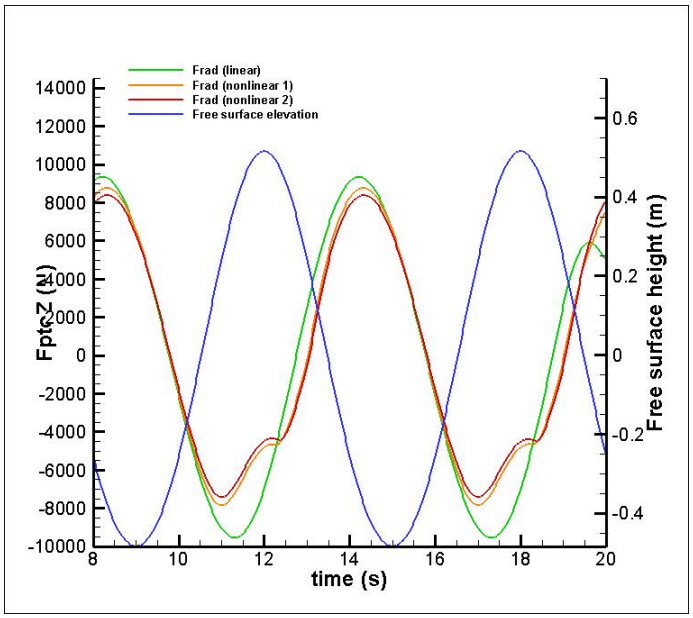

FIGURE 6. PTO FORCE

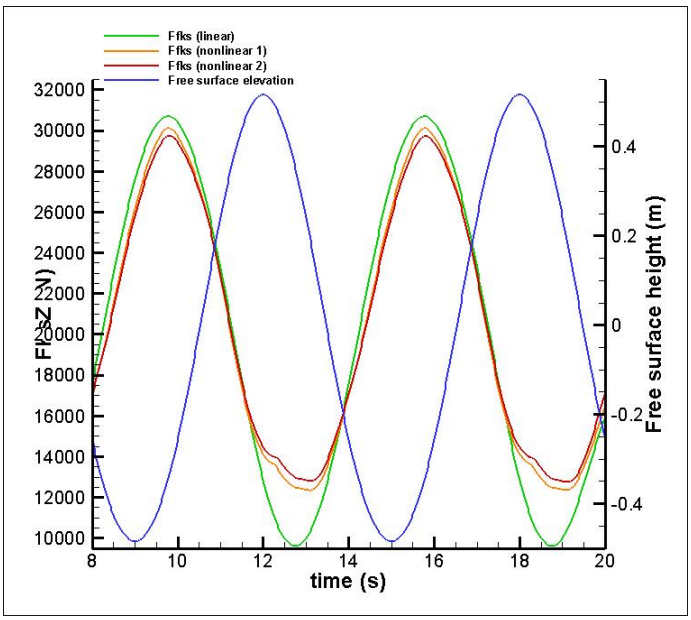

FIGURE 5. STATIC FROUDE-KRYLOV FORCE

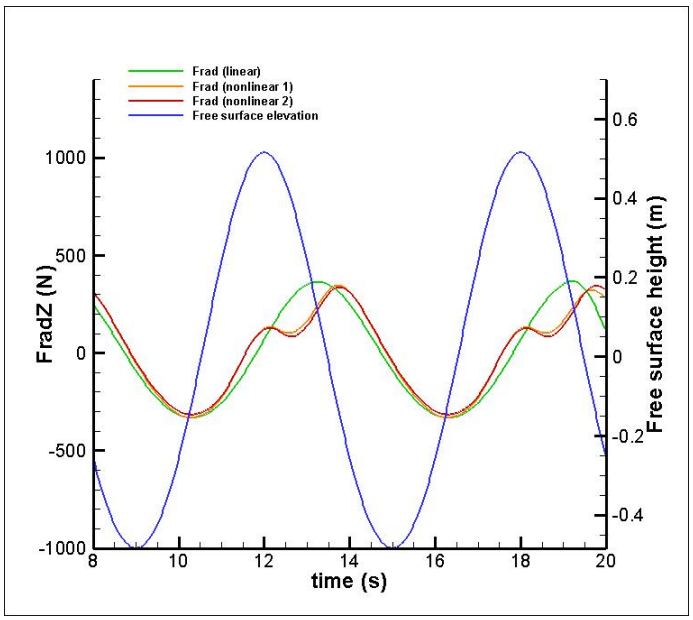

FIGURE 7. RADIATION FORCE

7.2 Power production

To examine the difference between linear and nonlinear modelling in terms of power production estimation, Fig.8 shows the difference in mean power estimation for the linear and nonlinear approaches. We note that there is significant overestimation of power production for the linear case and this becomes more exaggerated as the wave amplitude increases, as shown in Fig.9.

8 Conclusions

The computational requirements of the more complex nonlinear method (improvement 2) are hardly justified by any significant difference in results, compared to the nonlinear 1 formulation, considering the factor of 10 difference in computation time. We note that the nonlinear effects really start to become significant when the motion becomes large - this is exactly the

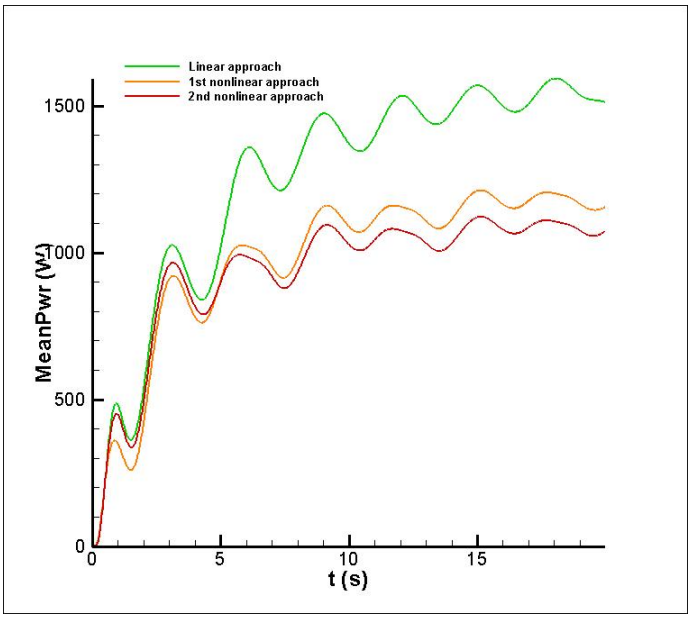

FIGURE 8. POWER PRODUCTION ESTIMATION FOR 0.5m WAVE AMPLITUDE

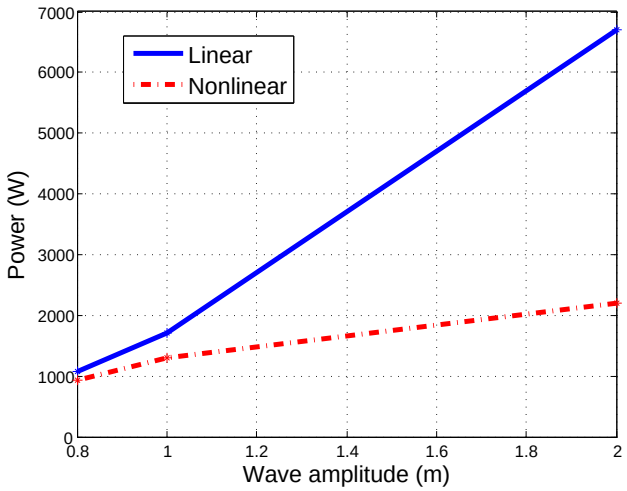

FIGURE 9. POWER PRODUCTION ESTIMATES FOR VARIOUS WAVE SIZES

situation which is aimed for in wave energy device operation! In particular, we can comment on the significance of the power production plot of Fig.9. Frequently, linear hydrodynamic methods are used to evaluate the power production figures for prototype devices. As the motion of wave energy devices becomes more significant, the tendency is for linear methods to overestimate the motion and, consequently, the power production. While there is, no doubt, a threshold beyond which devices may be taken out of power production mode (and put in a 'survival' mode), there is certainly a significant power production mode widow where motion will be large enough to cause considerable deviations between linear and nonlinear modelling approaches and therefore create the potential for overestimation of power production capability. There are also significant implications for wave energy device control design - overestimation of motion may cause controllers to be overly conservative or, at least, not respect the true nonlinear nature of the dynamics of wave energy devices.

REFERENCES

[1] Pizer, D., 1992. Numerical prediction of the performance of a solo duck. Tech. rep., University of Edinburgh.

[2] Falnes, J., 2002. *Ocean Waves and Oscillating Systems, Linear interactions including wave-energy extraction*, 1 ed. Cambridge University Press.

[3] Babarit, A., and Clement, A., 2006. "Shape optimisation of the SEAREV wave energy converter". In World Renewable Energy Congress IX.

[4] Payne, G., Taylor, J., Bruce, T., and Parkin, P., 2008. "Assessment of boundary element method for modelling of a free floating sloped wave energy device. part 2: Experimental validation". *Ocean Engineering,* ***35***, pp. 342–357.

[5] Durand, M., Babarit, A., Pettinotti, B., Quillard, O., Toularastel, J., and Clément, A., 2007. "Experimental validation of the performance SEAREV wave energy converter with real time latching control". In EWTEC, Porto.

[6] King, B., 1987. "Time-domain analysis of wave exciting forces on ships and bodies". PhD thesis, The University of Michigan.

[7] Gilloteaux, J.-C., 2007. "Simulation de mouvements de grande amplitude. application à la récupération de l'énergie des vagues.". PhD thesis, Ecole Centrale de Nantes.

[8] Guerinel, M., Alves, M., and Sarmento, A., 2011. "Nonlinear modelling of the dynamics of a free floating body". In EWTEC, Southampton.

[9] Bretl, J. G., 2009. "A time domain model for wave induced motions coupled to energy extraction.". PhD thesis, University of Michigan.

[10] Cummins, W., 1962. "The impulse response function and ship motions". *Schiffstechnik,* ***9***, pp. 101–109.

[11] Rienecker, M. M., and Fenton, J., 1981. "Fourier approximation method for steady water waves". *Journal Of Fluid Mechanics,* ***104***, pp. 119–137.